River inflow and retention time affecting spatial heterogeneity of chlorophyll and water-air CO_2 fluxes in a tropical hydropower reservoir.

F. S. Pacheco[1], M. C. S. Soares[2], A. T. Assireu[3], M. P. Curtarelli[4], F. Roland[2], G. Abril[5], J. L. Stech[4], P. C. Alvalá[1], J. P. Ometto[1]

[1] {Earth System Science Center, National Institute for Space Research, São José dos Campos, 12227-010, São Paulo, Brazil.}.

[2] {Laboratory of Aquatic Ecology, Federal University of Juiz de Fora, Juiz de Fora, 36036-900, Minas Gerais, Brazil.}

[3] {Institute of Natural Resources, Federal University of Itajubá, Itajubá, 37500-903, Minas Gerais, Brazil.}

[4] {Remote Sense Division, National Institute for Space Research, São José dos Campos, 12227-010, São Paulo, Brazil.}

[5] {Laboratoire Environnements et Paléoenvironnements Océaniques et Continentaux (EPOC), CNRS, Université Bordeaux 1, Avenue des Facultés, 33405 Talence, France}

Corresponding author e-mail: F. S. Pacheco (felipe.pacheco@inpe.br)

Abstract

Much research has been devoted to understanding the complexity of biogeochemical and physical processes responsible for the greenhouse gas (GHG) emissions from hydropower reservoirs. Spatial complexity and heterogeneity of GHG emission may be observed in these systems because it is dependent on flooded biomass, river inflow, primary production and dam operation. In this study, we investigated the relationships between the water-air CO_2 fluxes and the phytoplanktonic biomass in Funil Reservoir, an old, stratified tropical reservoir, where intense phytoplankton blooms and low partial pressure of CO_2 (pCO_2) are observed. Our results showed that the Funil Reservoir seasonal and spatial variability of chlorophyll concentration (Chl) and pCO_2 is more related to changes in the river inflow over the year than to environmental factors such as air temperature and solar radiation. Field data and hydrodynamic simulations reveal that the river inflow contributes to the increased heterogeneity in the dry season due to the variation of reservoir retention time and river temperature. Contradictory conclusions can be drawn if temporal data collected only near the dam is considered instead of spatial data to represent CO_2 fluxes in whole reservoir. During periods of high retention time, the average CO_2 fluxes were 10.3 mmol m^{-2} d^{-1} based on temporal data near the dam versus -7.2 mmol m^{-2} d^{-1} using spatial data collected along the reservoir surface. In this case, the use of temporal data alone to calculate the CO_2 fluxes results in the reservoir acting as a source instead of a sink of CO_2. This suggest that the lack of spatial data to calculate the C budgets in reservoirs can affect regional and global estimates. Our results support the idea that Funil Reservoir is a dynamic system where the hydrodynamics represented by changes in the river inflow and retention time is potentially a more important force driving both Chl and pCO_2 spatial variability than in-system ecological factors.

1 Introduction

Over the last two decades, hydropower reservoirs have been identified as potentially important sources of greenhouse gas (GHG) emissions (St Louis et al., 2000; Rosa et al., 2004; Demarty et al., 2011). In tropical region, high temperatures and the flooding of large amounts of biomass, including primary forest, result to intense GHG emission (Abril et al., 2005; Fearnside and Pueyo, 2012). However, emissions are larger in tropical Amazonian (Abril et al., 2013) than in tropical Cerrado reservoirs (Ometto et al., 2011) and in younger than in older reservoirs (Barros et al., 2011). Large hydroelectric reservoirs, especially those created by impounding rivers, are morphometrically complex and spatially heterogeneous (Roland et al., 2010;Teodoru et al., 2011; Zhao et al., 2013). Different regions in terms of CO_2 may be observed in these systems because it is dependent on flooded biomass, river input of organic matter, primary production and dam operation regime. Furthermore, both heterotrophic and autotrophic activity influences CO_2 concentration along reservoirs and the role of these activities has been reported in subtropical (Di Siervi et al., 1995), tropical (Roland et al., 2010; Kemenes et al., 2011) and temperate areas (Richardot et al., 2000; Lauster et al., 2006; Finlay et al., 2009; Halbedel and Koschorreck, 2013).

As the sedimentation and light availability increase along the reservoir, the biomass of primary producers may increase. The phytoplankton is distributed in patches along the reservoir due to differences in habitat conditions linked to nutrient distribution, light availability and stratification (Serra et al., 2007). Also, hydrodynamics factors as retention time and river inflow showed to influence the phytoplankton communities and growth (Vidal et al., 2012; Soares et al., 2008). Intense phytoplankton primary production has been identified as the main regulator of carbon (C) budget in temperate eutrophic lakes (Finlay et al., 2010; Pacheco et al., 2014), however the impact on tropical hydropower reservoir is still unclear.

River inflows may affect biogeochemical patterns in river valley reservoirs (Kennedy, 1999). Density differences of the incoming stream and lake water, stream and lake hydraulics, strength of stratification and mixing are features that control how the river water will flow when it reaches the reservoir (Fischer and Smith, 1983; Fischer et al., 1979). As result of density differences between river and lake water, the river enters in the lake and can flow large distances as a gravity-driven density current (Ford, 1990; Martin and McCutcheon, 1998). The interaction of large nutrient loads injected by river and the dynamic of river inflow can determine the spatial heterogeneity in

phytoplankton distribution (Vidal et al., 2012). Consequently, river inflow may affect primary production along river/dam axis in hydropower reservoirs strongly influenced by river.

In this study, we investigated the relationships between phytoplanktonic biomass and water-air CO_2 fluxes in an old, stratified tropical reservoir (Funil, state of RJ, Brazil), where intense phytoplankton blooms and low pCO_2 are observed in the water. We combine fieldwork and modeling to analyze the respective impact of meteorological and hydrological factors on the spatial and temporal dynamics of phytoplankton and the intensity of CO_2 fluxes. We show the effect of the river inflow in the heterogeneity of pCO_2 and Chl in Funil Reservoir. We also compare temporal data of pCO_2 collected near the dam with a high density of spatial data. Our hypothesis is that the seasonal and spatial variability of pCO_2 and Chl in Funil Reservoir is more related to river inflow and retention time than to external environmental factors such as air temperature and solar radiation. We highlight that very different conclusions can be drawn regarding carbon cycle in reservoirs if spatial heterogeneity is not adequately considered.

2 Materials and Methods

2.1. Study Site

Funil Reservoir is an old impoundment constructed at the end of the 1960s and is located on Paraíba do Sul River, in a southern city (Resende) of the Rio de Janeiro State, Brazil (22°30'S, 44°45'W, Fig. 1). It is 440 m above sea level, with wet-warm summers and dry-cold winters. The main purpose of Funil Reservoir is energy production, but the reservoir is also used for irrigation and recreation. It has a surface area of 40 km^2, mean and maximum depth of 22 and 74 m, respectively, and total volume of 890 x 10^6 m^3. The maximum and minimum reservoir water level occurs in the end of the rainy season (April) and dry season (October), respectively. From October 2011 to September 2012, the difference between minimum and maximum water level was 15.6 meters.

Funil Reservoir has a catchment area of 12,800 km^2 hosting one of the highest industrialized regions in Brazil. There are around 2 million people living inside the catchment area and 39 cities depending on the Paraíba do Sul River for water supply. These cities comprises 2% of Brazil's gross domestic product (GDP) (IBGE, 2010). In this area, 46% of sewage is untreated (AGEVAP,

2011) and the Paraiba do Sul River receives a large portion of the sewage from one of the most populated regions in Brazil (20-50 hab km^{-2}, IBGE, 2010). Consequently, the river has a large influence on the reservoir's water quality that has experienced tragic eutrophication in recent decades, resulting in frequent and intense cyanobacterial blooms (Klapper, 1998; Branco et al., 2002; Rocha et al., 2002). The river inflow is affected by the water supply-demand and operation of dams constructed upstream. In general, Funil Reservoir is a turbid, eutrophic system, with high phytoplankton (cyanobacteria) biomass (Soares et al., 2012; Rangel et al., 2012).

2.2. Field Sampling

Spatial data – the water samples for the determinations of the Chl and pCO_2 were taken between 9:00 to 12:00 Local Time (LT; UTC/GMT -3 hours) on 1 March 2012 (end of the rainy season, high water lever) and 20 September 2012 (end of the dry season, low water level). Samples were taken at the surface (0.3 m) at 42 stations in Funil Reservoir (28 located along the main body of the reservoir, Fig. 1) in the same day to limit the effect of diurnal variation on the results.

We measured the Chl using a compact version of PHYTO-PAM (Heinz Walz GmbH, PHYTO-ED, Effelrich, Germany). The pCO_2 data were determine using water-air equilibration method. In a marble-type equilibrator (Abril et al., 2014; Abril et al., 2006), the water pumped directly from the lake flows from the top to the bottom (0.8 liters per min), while a constant volume of air (0.4 liters per min) flows from the bottom to the top. The large gas exchange surface area promoted by the contact with the marbles accelerates the pCO_2 water-air equilibrium. The air pump conduct the air from the top of the equilibrator through a drying tube containing a desiccant (Drierite), then to an infrared gas analyzer (IRGA, LI-840, LICOR, Lincoln, Nebraska, USA), and then back to the bottom of the equilibrator (closed air circuit, Abril et al., 2006). For each station, the lake water and air were pumped through this system for two minutes before the pCO_2 from the IRGA stabilized to a constant value.

Color maps were created to represent the spatial distribution of Chl and pCO_2 (Fig. 2). We used the variogram analysis to describe the spatial correlation among samples and to spatially interpolate using Kriging methods (Bailey and Gatrell, 1995). The empirical variograms were fitted to different mathematical models using the Akaike's information criterion (AIC, Akaike, 1974) to evaluate the best fit. The best model variogram were used for interpolation by ordinary

kriging. We used the software Spring (Câmara et al., 1996) version 5.1.8 to conduct the spatial analysis and to produce the in situ pCO_2 and Chl maps.

In this study, we used the Chl as a parameter to separate the reservoir in three zones. Riverine zone was characterized by low Chl (<5 $\mu g\ L^{-1}$). Transition zone begins where the Chl starts to increase (>5 $\mu g\ L^{-1}$) and ends when the Chl decrease to levels closely to the Chl in Lacustrine zone (<60 $\mu g\ L^{-1}$). Finally, the Lacustrine zone is characterized by intermediate Chl (>5 and <60 $\mu g\ L^{-1}$); however picks of Chl were observed in some regions of the Lacustrine zone. We estimated the size of each zone (riverine, transition, lacustrine) of the reservoir in the dry and rainy seasons using the results from the spatial interpolation of the Chl data. After the interpolation, we used a pixel classification method to determine the boundaries of each zone (class). We checked the boundary locations with the observed data. Finally, we determined the area multiplying the number of pixels of each class by the area of each pixel. The boundary of each zone is represented in the maps (Fig. 2) by the dashed lines.

Time series data - Wind speed and direction, solar radiation, pH, dissolved oxygen (DO), air temperature and temperature profiles (2 m, 5 m, 20 m and 40 m depth) were collected hourly at station S28 near the dam (Fig. 1) and transmitted by satellite in quasi-real time by the Integrated System for Environmental Monitoring (SIMA). The SIMA is a set of hardware and software developed for data acquisition and real-time monitoring of hydrological systems (Alcantara et al., 2013;Stevenson et al., 1993). The SIMA consists of an independent system formed by an anchored buoy containing data storage systems, sensors (air temperature, wind direction and intensity, pressure, incoming and reflected radiation and a thermistor chain), a solar panel, a battery and a transmission antenna. A sonde (YSI model 6600, Yellow Spring, Ohio, USA) was attached to the SIMA buoy to collect hourly surface data on temperature, conductivity, pH, and oxygen. This sonde was calibrated every 15 days according to the YSI Environmental Operations Manual (http://www.ysi.com/ysi/support).

We calculated the pCO_2 in the surface water over one year near the dam from measured pH and alkalinity. The calculations include dependence on temperature for dissociation constants of carbonic acid (Millero et al., 2002) and solubility of CO_2. We used pH and temperature collected by SIMA between 25 October 2011 and 25 October 2012 and monthly data of alkalinity determined by the titration method (APHA, 2005) at station S28 (Fig. 1). Samples for total

phosphorous (TP) and nitrogen (TN) were taken monthly. For TP, the samples were oxidized by persulfate and then analyzed as soluble reactive phosphorus. TN was determined as the sum of organic fraction measured by Kjedahl method and the dissolved inorganic nutrients. Laboratory analysis for TP and NP was performed according to standard spectrophotometric techniques (Wetzel and Likens, 2010).

2.3. CO_2 flux calculation

The air-water flux of CO_2 (mmol m^{-2} d^{-1}) was calculated according to Eq. (1). Positive values of CO2 fluxes denotes net gas flux from the lake to the atmosphere

$$F(CO_2) = k\alpha\Delta pCO_2 \quad (1)$$

Where k is the gas transfer velocity of CO_2 (in m h^{-1}), α is the solubility coefficient of CO_2 (in mmol m^{-3} μatm^{-1}) as a function of water temperature (Weiss, 1974), and ΔpCO_2 is the air-water gradient of pCO_2 (in μatm). The atmospheric pCO_2 measured in the rainy and dry season was 375 μatm and this atmospheric value was used for all flux calculation. The gas transfer velocity k was calculated from the gas transfer velocity normalized to a Schmidt number of 600 (k_{600}) that corresponds to CO_2 at 20 °C (Eq. 2) (Jahne et al., 1987).

$$k = k_{600}\left(\frac{Sc}{600}\right)^{-0,5} \quad (2)$$

Where Sc is the Schmidt number of a given gas at a given temperature (Wanninkhof, 1992). k_{600} is the normalized gas transfer velocity calculated from wind speed (MacIntyre et al. 2010) using different equations under cooling and heating conditions (Eq. 3, 4). We also evaluated a wind-speed formulation by Cole and Caraco (1998) to investigate the importance of different formulation of k_{600} (Eq. 5). A more detailed description for these equations is in Staehr et al. (2012). The k_{600} was calculated in cm h^{-1} and converted to m d^{-1}.

$$k_{600} = 2.04U_{10} + 2.0 \quad \text{(under cooling, MacIntyre et al. 2010)} \quad (4)$$

$$k_{600} = 1.74U_{10} - 0.15 \quad \text{(under heating, MacIntyre et al. 2010)} \quad (5)$$

$$k_{600} = 2.07 + 0.21\,U_{10}^{1.7} \quad \text{(Cole and Caraco 1998)} \quad (6)$$

Where U_{10} is wind speed at 10 meters height. The wind speed was obtained from the SIMA da at 3 meters height and was calculated for 10 meters height (Smith, 1985).

In riverine zone, we considered the k_{600} as a function of wind and water current. The contribution of the water current to the gas transfer velocity was estimated using the water current (w, cm s^{-1}), depth (h, meters) and the equations in Borges et al. (2004) (Eq. 6)

$$k_{600} = 1.719 w^{0.5} h^{-0.5} \quad (6)$$

2.4. Temperature profile

Temperature profiles were collected using thermistor chain deployed at the station S09 in the rainy season and station S14 in the dry season to determine the thermal structure at the transition zone. Eleven thermistors (Hobo, U22 Water Temp Pro v2, Bourne, Massachusetts, USA) were placed every 0.5 m up to 4 meters and every 1 m from 5 to 7 meters. We also deployed a thermistor chain at the riverine zone at the station S05 with thermistors placed every 2 meter. The thermistors were programed to record temperature every 10 minutes. In the rainy season, the thermistor chain was deployed on 29 February 2012 at 18:30 LT and recovered after 40 hours. In the dry season, the thermistor chain was deployed on 20 September 2012 at 11:30 LT and recovered after 25 hours.

In our analysis, temperature is considered as the factor controlling water density. The use of temperature is justified by the low conductivity and turbidity in the river. The values of turbidity measured in the field of 29 and 11 NTU in the rainy and dry seasons, respectively, would have affected density <5% relative to that of temperature (Gippel, 1989).

2.5. Numerical Model description and setup

Numerical simulations of the lake hydrodynamics were conducted with the Estuary and Lake Computer Model (ELCOM, Hodges et al., 2000). This model solves the 3D hydrostatic, Boussinesq, Reynolds-averaged Navier–Stokes and scalar transport equations, separating mixing of scalars and momentum from advection. The hydrodynamic algorithms that are implemented in the ELCOM use an Euler-Lagrange approach for the advection of momentum adapted from the work of Casulli and Cheng (1992), whereas the advection of scalars (i.e., tracers, conductivity and temperature) is based on the ULTIMATE QUICKEST method proposed by Leonard (1991). The thermodynamics model considers the penetrative (i.e., shortwave radiation) and non-penetrative

components (i.e., longwave radiation, sensible and latent heat fluxes) (Hodges et al., 2000). The vertical mixing model uses the transport equations of turbulent kinetic energy (TKE) to compute the energy available from wind stirring and shear production for the mixing process (Spigel and Imberger, 1980). A complete description of the formulae and numerical methods used in the ELCOM was given by Hodges et al. (2000).

Hydrodynamic simulations of Funil Reservoir were conducted with realistic forcing condition (e.g. inflow, outflow, atmospheric temperature, radiation). These simulations were aimed in order to test the hypothesis regarding the river inflows at transition zone in the rainy and dry seasons in Funil Reservoir. Simulations started 4 days before the date of the considered data. This is necessary to let the model equilibrate beyond the initial physical conditions. The digital representation of the reservoir bathymetry (numerical domain) was defined based on the bathymetric data collected from 27 to 29 February 2012. The numerical domain was discretized in a uniform horizontal grid containing 100 m x 100 m cells. The vertical grid resolution was set to a uniform 1 m thickness, resulting in 72 vertical layers. The water albedo was set to 0.03 (Slater, 1980), and the bottom drag coefficient was set to 0.001 (Wüest and Lorke, 2003). The attenuation coefficient for PAR was set to 0.6 m^{-1} based on Secchi disc measurements. Based on a previous study conducted in another tropical reservoir (Pacheco et al., 2011), a value of 5.25 m^2 s^{-1} was chosen for the horizontal diffusivity for temperature and for the horizontal momentum.

Because of the presence of persistent unstable atmospheric conditions over tropical reservoirs (Verburg and Antenucci, 2010), the atmospheric stability sub-model was activated during the simulation; this procedure is adequate since the meteorological sensors are placed within the atmospheric boundary layer (ABL) over the surface of the lake and data are collected at sub-daily intervals (Imberger and Patterson, 1990). In this manner, at each model time step the heat and momentum transfer coefficients were adjusted based on the stability of the ABL. The stability of ABL is evaluated through the stability parameter, derived from the Monin-Obukhov length scale. ELCOM uses the similarity functions presented in Imberger and Patterson (1990) for both cases, stable (negative values stability parameter) and unstable conditions (positive values). The Coriolis sub-model was also activated during the simulation and then Coriolis force was considered in the Navier-Stokes equation. This force causes the deflection of moving objects (in this case the water currents) when they are viewed in a rotating reference frame (e.g. the Earth).

We defined two sets of boundary cells to force the inflow (Paraíba do Sul River) and outflow: (the water intake at the dam). The meteorological driving forces over the free surface of the reservoir were considered uniform. The model was forced using hourly meteorological data acquired by SIMA, the daily inflow and outflow provided by Eletrobrás-Furnas and river temperatures extracted from thermistor chain data. In order to complement the data of river temperature, we used the M*D11A1 L3 product (Wan, 2008), obtained from the National Aeronautics and Space Administration Land Processes Distributed Active Archive Center. The M*D11A1 is a standard products, generated using a split-window algorithm and seven spectral MODIS bands located in the regions of the shortwave infrared and thermal infrared. This algorithm is based on the differential absorption of adjacent bands in the infrared region (Wan and Dozier, 1996). The M*D11A1 products have been validated at Stage 2 by a series of field campaigns conducted between 2000-2007, and over more locations and time periods through radiance-based validation studies. Accuracy is better than 1 °C (0.5 °C in most cases). This product is generated up to four times each day (i.e., 10:30 h, 13:30 h, 23:30 h and 2:30 h) and is delivered in a georeferenced grid with 1 km of spatial resolution in a sinusoidal projection.

The cloud cover fraction over Funil Reservoir was retrieved using MODIS Level 2 Cloud Mask product (named M*D35L2) (Ackerman et al., 1998).The algorithm used to generate this product employ a series of visible and infrared threshold and consistency tests to specify confidence that an unobstructed view of the Earth's surface is observed. This product is generated up to four times each day (i.e., 10:30 h, 13:30 h, 23:30 h and 2:30 h) and is delivered in a georeferenced grid with 1 km of spatial resolution in a sinusoidal projection.

The MODIS products were acquired online (http://reverb.echo.nasa.gov/reverb/) and preprocessed using the MODIS Reprojection Tool (available at https://lpdaac.usgs.gov). The data were first resampled to a 100 m spatial resolution (compatible with the bathymetric grid). They were then re-projected to the Universal Transverse Mercator (UTM) coordinate system (zone 22 South) with the World Geodetic System (WGS-84) datum as reference; they were then converted to a raster image. Finally, a MATLAB® program was then used to retrieve the temperature at the rivers inflows and to compute the cloud cover fraction over the reservoir.

Two periods were simulated: one to represent the rainy season (25 February 2012 to 4 March 2012) and one to represent the dry season (15 to 23 September 2012).

3 Results

3.1. Spatial variability

Based on the spatial data of Chl and pCO_2, a typical zonation pattern usually found in reservoirs was observed in Funil main body (riverine, transition and lacustrine zones) (Fig 2). Although the boundaries are influenced by many factors and are not easily determined, these regions have distinct physical, chemical and biological features. The riverine zone (RZ) has a high input of nutrients coming from terrestrial systems and human activities, but the primary production is limited by high turbidity and turbulence. As the sedimentation and light availability increase along the reservoir, biomass of primary producers increases in the transition zone (TZ). The lacustrine zone (LZ) is characterized by nutrient limitation and reduced phytoplankton biomass (Thornton 1990).

Funil Reservoir showed to be spatially heterogeneous with seasonal differences in Chl and pCO_2 (Fig. 2). The spatial data showed high spatial variation only in the main body of the reservoir, while the southern part was undersaturated in CO_2 in the rainy and dry seasons (Fig 2a, b). Spatially average of pCO_2 for the rainy and dry season were 259 ± 221 and 881 ± 900 μatm, respectively. The pCO_2 varied from 140 to 1376 μatm in the rainy season and from 43 to 2290 μatm in the dry season. Higher values of pCO_2 in the riverine zone of the reservoir and a drastically decrease in the transition zone were observed in both sample periods (Fig. 3a,b). In the lacustrine zone, undersaturation on CO_2 was prevalent at all sample sites in the rainy and dry season. Considering all sample sites, there was significant differences between the rainy and dry seasons ($t = 1.99$, $p < 0.05$) and higher values of pCO_2 during the dry season in Funil Reservoir were previously reported (Roland et al., 2010). The Chl were similar in the transition and lacustrine zone in the rainy season ($t = 2.01$, $p > 0.05$) and higher in the transition zone in the dry season ($t = 2.01$, $p < 0.05$, Fig. 3a,b; Table 1). Further, average concentration in transition zone was 2.5 times higher than the reservoir average (129.2 and 52.0 μg L^{-1}, respectively). Unlike pCO_2, Chl data showed no significant difference between the rainy and dry season considering all spatial data ($t = 1.99$, $p > 0.05$).

The calculated CO_2 fluxes from spatial data varied from -46.5 to 52.2 mmol m^{-2} d^{-1} and -61.9 to 103.16 mmol m^{-2} d^{-1} in the rainy and dry season, respectively. In both the rainy and dry seasons, the maximum emission was observed in riverine zone and the minimum in the transition zone. The spatial average was -10.1 and 24.6 mmol m^{-2} d^{-1} in the rainy and dry season, respectively (Table 1).

3.2. Temporal variability

The pCO_2 calculated by multi-parameter sonde data (temperature and pH) and alkalinity showed a large seasonal variability over the year at the station near the dam (Table 2). The pCO_2 varied from 35 to 4058 μatm with average of 624 ± 829 μatm and median of 165 μatm. The pCO_2 supersaturation was prevalent between April and June, while pCO_2 undersaturation was prevalent in all other periods (Fig 4a). Lowest median of pCO_2 was observed between October and December (43 μatm). Considering all temporal data over the year, 59.8% of the data were below atmospheric equilibrium and 1.1% were within 5% of atmospheric equilibrium.

In Funil Reservoir, the seasonal pCO_2 variation over the year at the station near the dam agreed with variation of retention time (Fig. 4). The yearly average of the reservoir retention time was 32.6 days over the considered year. Lower retention time occurs between October and December when the water level is low and the reservoir is ready to stock water coming from the watershed and rain during the rainy season (October to March).

Since we sampled temperature in a sub-daily scale over the year, we assumed the equations proposed by MacIntyre et al. (2010) to calculate k_{600} that also consider the turbulence from heat loss. The turbulence from heat loss especially overnight often exceeds that from wind mixing in tropical lakes that tends to have low winds. However, the differences between estimates did not significantly changed our results (Table 1). The CO_2 flux over the year at the station near the dam varied from –104.7 to 175.88 mmol m^{-2} d^{-1}. The average of flux was -0.1 ± 39.8 mmol m^{-2} d^{-1} and median was -7.4 mmol m^{-2} d^{-1}. We observed substantial uptake of CO_2 between October and December (rainy-spring) (Table 1). From January to July, the lake lost substantial CO_2 via degassing (Table 1). Uptake of CO_2 from the atmosphere was also prevalent between July and September (dry-winter). Summary of all other data collected over the studied period is shown in Table 2.

CO_2 fluxes estimated from two different equation of k_{600} (see Methods) were not significantly different for the spatialized data ($t = 1.99$, $p > 0.05$, Table 1). Due to the large sample size of the temporal data (hourly data), significant difference was observed between the estimates, mainly in the dry-autumn when the surface temperature decreased after the warm-summer ($t = 1.96$, $p < 0.05$).

3.3. Thermal structure of transition zone and river

During the rainy season, thermal stratification occurred in the transition zone only during the daytime around 16:30 LT, when a maximum of 33.1 °C was observed at the surface for a minimum of 27.8 °C at the bottom (Fig. 5a); to the contrary, temperature was vertically homogeneous at nighttime. The daily range of temperature oscillation during the rainy season at surface was up to 5 °C. In the dry season, water temperature was lower compared to the rainy season at transition zone. Stratification occurred around 14:00 LT in dry season, when we observed a maximum of 25.7 °C and a minimum of 23.1 °C at the bottom. The daily range of temperature oscillation was up to 3°C at surface and stratus layers with different temperatures were observed every 2.5 meters (Fig. 5b). The river temperature varied from 27.7 to 28.7 °C and 23.6 to 24.1 °C in the rainy and dry season, respectively (Table 3). The average temperature difference between river and reservoir surface water was 2.1 and 0.3 °C in the rainy and dry season, respectively.

3.4. Simulations

We first compared the simulated and real temperature at station S09 and S14 for the rainy and dry season, respectively. The RMSE calculated by comparing the data every 20 minutes were 1.4 °C for the rainy season and 1.1°C for the dry season. These results obtained for both seasons were comparable with previous modelling exercises found in literature (Jin et al., 2000, Vidal et al., 2012). We also analyzed the ability of the model to reproduce the inflow using data from drifters released in the river and transition zone of the reservoir on 1 March and 20 September (data not shown). Although the vertical thermal structures observed in the dry season (Fig. 5b) were not well represented, the model reproduced the behavior of the inflow as underflow in the rainy season (Fig. 6a) and interflow and overflow in the dry season (Fig. 6b) as anticipated by the schematic representation (Fig. 5c,d). The river flowed mainly at 6 meters depth near the bottom of Funil

Reservoir after the river plunging point in the rainy season. In the dry season, the river flowed mainly at 3 meters depth at night and 4 meters at daytime.

The daily oscillation of the neutral buoyance observed occurs because of the variation of reservoir surface and river temperatures (Vidal et al. 2012, Curtarelli et al. 2013). The level of neutral buoyancy, where the densities of the flowing current and the ambient fluid are equal, represents the depth where the river water spreads laterally in the reservoir. In the rainy season, the river flowed as underflow (Fig. 6a), however, when the river reached its maximum temperature around 21:00 LT (Table 3) the temperature difference between river and surface water decreased, the level of river neutral buoyance moved upward and the maximum flow was observed between 4 and 6 meters (Fig. 6a). In the dry season, the river flowed as overflow, but it plunged down to 4 to 6 meters depth when the high surface temperature during the day coincided with the period of lowest river temperature (Table 3) and neutral buoyance moved downward (Fig. 6b). The change in patterns observed in the river flow between 20 and 21 September occurred due to a decrease of the river temperature during a rainfall that occurred around 16:00 LT on 20 September 2012 (Fig. 6b).

4 Discussion

4.1. pCO_2 driven by Phytoplankton

Primary production associated with high Chl showed to be the main regulator of CO_2 concentration at the surface of Funil Reservoir (Fig. 7). Spatially, the pCO_2 were negatively correlated with the Chl ($r2 = 0.71$). In old hydropower reservoirs where C source from the flooded soil after impounding has become negligible, primary production may become a significant term in the C budget. Intense primary production fuelled by high levels of nutrients reduces CO_2 concentrations to levels below atmospheric equilibrium in transition and lacustrine zone of Funil Reservoir (Fig. 3). The high pCO_2 in the riverine zone may be explained by the terrestrial ecosystem respiration entering the river as dissolved soil CO_2, the oxidation of allochthonous and emergent autochthonous organic carbon, the acidification of buffered waters, the precipitation of carbonate minerals, and the direct pumping of root respiration CO_2 from riparian vegetation (Butman & Raymond, 2011).

Low pCO_2 levels observed at the station near the dam over the year is associated with (1) high primary production due to higher temperature and solar radiation that promote water column stability and stratification, and (2) constant high nutrient availability. Since nutrient availability in Funil Reservoir is high during the entire year (Table 2), phytoplankton growth is not limited by nutrients in the lacustrine zone. However, seasonal variation of factors that controls stability and stratification, such as temperature, wind and mixing zone depth may inhibit algal growth near the dam especially between April and June.

Due to phytoplankton productivity, we observed net uptake of CO_2 over the year at the station near the dam, especially between October and December (Table 1). However, the fate of carbon fixed by the phytoplankton in Funil Reservoir is still unclear. The higher flux of methane (CH_4) from sediment to water found in Funil Reservoir compared to other tropical reservoir (Ometto et al., 2013) suggests that a substantial fraction of the carbon fixed by the phytoplankton reaches the sediment and is further mineralized in CH_4. However, in the lacustrine zone, the higher depth and high temperature may promote the decomposition of dead phytoplankton generating CO_2 or CH_4 in the water column before it reaches the sediment.

It is important to point out that the CO_2 production in the sediments can leave an imprint in the pCO_2 of the surface water especially in the dry season when the reservoir is not stratified. During periods of water stratification, the carbon coming from the organic carbon mineralization in the sediment may be trapped in the hypolimnion and may not contribute to the CO_2 flux from the water to the atmosphere (Cardoso et al., 2013). In addition, it is important to highlight that the contribution of the carbon mineralization in the sediment to the pCO_2 in the surface can also be regulated by other factors such as the CO_2 saturation in the water and depth of the reservoir (Guérin et al.,2006). Moreover, when the river plunges and flows at the bottom of the reservoir, the water flow can disturb the sediment and enhance the carbon flux from the sediment to the hypolimnion, which can affect the contribution of the organic carbon mineralized on the sediment to the amount of carbon emitted by the reservoir.

By considering that the outflow exported the same amount of carbon that came from the watershed (Table 2), we suggest that a high sedimentation rate offset the uptake of CO_2 from the atmosphere to close the carbon budget. Although there is no data to support this statement, we hypothesize that the burial of organic carbon composed by phytoplankton and methanogenesis could be two

important carbon pathways for the carbon fixed by the phytoplankton in Funil Reservoir, as reported in natural eutrophic lakes (Downing et al., 2008).

4.2. Physical feature and spatial distribution

Funil Reservoir retention time is strongly driven by the operation of the dam. The volume of water that flows through the turbine depends on the energy demands and inflow from Paraiba do Sul River. Periods of low retention time and water levels do not necessarily correspond to periods of low precipitation. In fact, the highest retention time and water level is often observed in the middle of the dry season when the reservoir is full to ensure enough water to produce energy during entire dry season. This suggest that not only natural factors are driving processes, but also it may be regulated by the dam operation in Funil Reservoir.

The position of the transition zone of the reservoir moves as a result of the season (Fig.3). In the end of the rainy season, the retention time and water level was high, and the influence of the river in the surface water of the reservoir was restricted to a small area (Fig. 2a, c). Contrarily, when the water level and retention time was low, the transition zone moved toward the dam and the river inflow influenced the surface Chl and pCO_2 in more than 40% of the total reservoir surface area (Fig. 2b, d). As previously reported, when retention time is short, a reservoir can become a fluvial-dominated system (Straškraba, 1990).

Size of the river-influenced area in the reservoir surface water also depends on the water density. Differences on river and reservoir temperature, total dissolved solids, and suspended solids can cause a density gradient in the water column. Depending on the water density differences between the inflow and reservoir, the river can flow into the downstream area as overflow, underflow, or interflow (Martin and McCutcheon, 1998). During the rainy season in Funil Reservoir, due to the high difference between river and reservoir surface temperature (~4 °C), the river water progressively sinks down (underflow), and contributes to the thermal stability of the water column (Fig. 5a, Assireu et al., 2011). The denser river water flows under the lighter reservoir water and waves and billows develops along the interface due to shear velocity. This behavior is indicative of the Kelvin-Helmholtz instability, in which waves made up of fluid from the current (river) promote mixing with the reservoir water (Thorpe and Jiang, 1998; Corcos and Sherman, 2005)

(Fig. 5c). This mixing and the high nutrient concentration coming from Paraíba do Sul River (Table 2) may explain the high Chl observed in the transition zone (Fig. 3).

Many cold fronts pass through Brazilian middle-west and southeast in the dry seasons. (Lorenzzetti et al., 2005, Alcântara et al., 2010). Thus, the decrease of reservoir surface temperature (Table 2) and consequent decrease in density difference between river and reservoir surface leads to river inflow characterized by inter-overflow (Fig. 5b,d). In an inter-overflow, the riverine characteristic of high turbulence, pCO_2 and low Chl is observed in the reservoir surface 5 kilometers toward the dam (Fig. 3a,b). Although there are high nutrient concentrations in the transition zone (Table 1) between S19 and the river, the surface water is dominated by river flow with low Chl concentrations (Fig. 3). Favorable conditions for phytoplankton blooming will only exist down-reservoir in the transition zone where the inflow mixes with the reservoir and loses velocity (Vidal et al., 2012).

The simulation of the rainy season (Fig. 6) showed low influence of the river inflow in the surface water, suggested by the thermal stability at transition zone (Fig. 5a). The simulation of the dry season represented the overflow, especially at night (Fig. 6b). However, the simulation did not represent the intrusions of the river water on different depths (every 2.5 m) suggested by temperature profile at transition zone (Fig. 5b). The variation of the river inflow over the day (Fig. 6) occurs as response of the lagged change in temperature of the river and reservoir. In the rainy season, this oscillation enhanced the intake of nutrients in the euphotic zone when the reservoir surface temperature decreases and the river temperature reaches its maximum in the end of the day (Table 3). During the day, when the river temperature drops, the large peak of Chl in transition zone (Fig. 3a) could be result of diurnal stratification developing (Fig. 5). In the dry season, the peak of Chl occurs five kilometers further downstream (Fig. 3b), since inflow never plunges due to lower temperature differences between river and reservoir surface.

4.3. Spatial and temporal heterogeneity

As a result of the phytoplankton growth associated with these physical features, there are large spatial and temporal variation of CO_2 fluxes in the Funil Reservoir. Several studies of hydropower reservoir have suggested that significant CO_2 evade from these systems to the atmosphere at a global scale (St Louis et al., 2000; Roehm and Tremblay, 2006; Barros et al., 2011; Fearnside and

Pueyo, 2012). However, recent studies have shown that the growing nutrient enrichment caused by human activities (eutrophication) can reverse this pattern in some hydropower reservoirs (Roland et al., 2010) and natural lakes (Pacheco et al., 2014). Our study shows that Funil Reservoir is spatially heterogeneous with high CO_2 emission in riverine zone and high CO_2 uptake in transition and lacustrine zone. Temporally, the reservoir near the dam is undersaturated in pCO_2 mainly between October and December, and supersaturated in pCO_2 between April and June (Table 1).

We might have different or opposite conclusions if the spatial and temporal pCO_2 data are analyzed separately. Previous studies suggested that in natural small lakes, a single sample site should be adequate to determine if a lake is above or below equilibrium with the atmosphere and the intensity of the fluxes (Kelly et al., 2001). However, large spatial heterogeneity, regarding pCO_2 and CO_2 emission to atmosphere, was observed in boreal (Teodoru et al., 2011) and tropical (Roland et al., 2010) reservoir. Our temporal data at the dam station showed lower pCO_2 over October, November and December when the retention time is extremely low (Table 4), but this observation does not represent the entire reservoir. The spatial data collected at low water level showed low pCO_2 in the dam as well, however almost half reservoir is supersaturated due to the river influence (Fig 2d). The average pCO_2 during low retention time was 881 μatm considering whole reservoir area, contrasting with only 69 μatm near the dam. Furthermore, if we considered only one station near the dam to estimate CO_2 flux between the lake surface and atmosphere, the conclusion would be contradictory. For example, in periods of low retention time, calculated CO_2 flux showed that CO_2 flux would be -17.6 mmol m^{-2} d^{-1} (CO_2 sink) considering one spot temporal data, and 22.1 mmol m^{-2} d^{-1} (CO_2 source) considering whole reservoir (Table 4).

Same contradictory conclusion can be found when studies with low number of sample sites are considered in the spatial heterogeneity discussion. Previous studies looking at the heterogeneity in Funil Reservoir showed no peak of phytoplankton biomass in the transition zone (Soares et al., 2012). In our study, the Chl data collected every 1000 meters as proxy were able to show a clear transition zone within the reservoir. Additionally, data analysis in Soares et al (2012), considering four sampling stations, showed that high spatial heterogeneity occurs in periods of high retention time (high water level). Contrastingly, we showed high spatial heterogeneity in low retention time, corresponding to periods with high influence of the river in the surface water. Thus, different

conclusions found by Soares et al. (2012) may be explained by the variation in the spatial distribution of transition zone location, once retention time and inflow are key parameters defining its location (Fig. 2c,d).

5 Conclusion

In summary, the seasonal and spatial variability of Chl and CO_2 fluxes in Funil Reservoir is mainly related to river inflow and retention time. However, the relationship between pCO_2 and Chl suggests that primary production regulates surface CO_2 fluxes in transition and lacustrine zone. Average of spatial data showed CO_2 evasion to the atmosphere in periods of low retention time (even with higher Chl) due to river influence on water surface, and CO_2 uptake in periods of high retention time when the river plunges and flows under the reservoir. However, the threshold of retention time that seal the transition between source and sink of CO_2 could not be determined. Comparison between spatial (42 stations) and temporal data (one station) showed that different conclusions can be drawn if spatial heterogeneity is not adequately considered. Moreover, the change of the transition zone location over the year must be considered when low number of stations is used to represent the spatial heterogeneity. The lack of spatial information of CO_2 flux could lead to erroneous conclusion of the importance of hydropower reservoirs to freshwater carbon cycle. Funil Reservoir is a dynamic system where the hydrodynamics linked to the river inflow and retention time controls both pCO_2 and Chl spatial variability and seems to be the key that regulate most of ecological process.

Acknowledgments

This work was supported by the project “Carbon Budgets of Hydroelectric Reservoirs of Furnas Centrais Elétricas S. A.”. Thanks to the Center for Water Research (CWR) and its director, Jörg Imberger, for making ELCOM available for this study. We also thank the São Paulo State Science Foundation for financial support (FAPESP process no. 2010/06869-0). GA is a visiting special researcher from the Brazilian CNPq program Ciência Sem Fronteiras (process #401726/2012-6).

References

Abril, G., Guerin, F., Richard, S., Delmas, R., Galy-Lacaux, C., Gosse, P., Tremblay, A., Varfalvy, L., Dos Santos, M. A., and Matvienko, B.: Carbon dioxide and methane emissions and the carbon budget of a 10-year old tropical reservoir (Petit Saut, French Guiana), Global Biogeochem Cy, 19, GB4007, doi: 10.1029/2005gb002457, 2005.

Abril, G., Richard, S., and Guerin, F.: In situ measurements of dissolved gases (CO_2 and CH_4) in a wide range of concentrations in a tropical reservoir using an equilibrator, Sci Total Environ, 354, 246-251, doi: 10.1016/j.scitotenv.2005.12.051, 2006.

Abril, G., Parize, M., Perez, M. A. P., and Filizola, N.: Wood decomposition in Amazonian hydropower reservoirs: An additional source of greenhouse gases, J. S. Am. Earth Sci., 44, 104-107, doi: 10.1016/j.jsames.2012.11.007, 2013.

Abril, G., Martinez, J.-M., Artigas, L. F., Moreira-Turcq, P., Benedetti, M. F., Vidal, L., Meziane, T., Kim, J.-H., Bernardes, M. C., Savoye, N., Deborde, J., Souza, E. L., Alberic, P., Landim de Souza, M. F., and Roland, F.: Amazon River carbon dioxide outgassing fuelled by wetlands, Nature, 505, 395-398, doi: 10.1038/nature12797, 2014.

Ackerman, S. A., Strabala, K. I., Menzel, W. P., Frey, R. A., Moeller, C. C., and Gumley, L. E.: Discriminating clear sky from clouds with MODIS, Journal of Geophysical Research: Atmospheres, 103, 32141-32157, 10.1029/1998JD200032, 1998.

AGEVAP: Relatório Técnico - Bacia do Rio Paraíba Do Sul - Subsídios às Ações de Melhoria da Gestão 2011, Associação Pró-Gestão das Águas da Bacia Hidrográfica do Rio Paraíba do Sul, 255, Resende, 2011.

Akaike, H.: New look at statistical-model identification, IEEE T. Automat. Contr., AC19, 716-723, doi: 10.1109/tac.1974.1100705, 1974.

Alcantara, E., Curtarelli, M., Ogashawara, I., Stech, J., and Souza, A.: Hydrographic observations at SIMA station Itumbiara in 2013, in: Long-term environmental time series of continuously collected data in hydroelectric reservoirs in Brazil, edited by: Alcantara, E., Curtarelli, M., Ogashawara, I., Stech, J., and Souza, A., PANGAEA, Bremerhaven, 1-3, 2013.

Alcântara, E. H., Bonnet, M. P., Assireu, A. T., Stech, J. L., Novo, E. M. L. M., and Lorenzzetti, J. A.: On the water thermal response to the passage of cold fronts: initial results for Itumbiara

reservoir (Brazil), Hydrol. Earth Syst. Sci. Discuss., 7, 9437-9465, doi: 10.5194/hessd-7-9437-2010, 2010.

APHA: Standard Methods for the Examination of Water and Wastewater, 21 ed., Washington, DC, 1368 pp., 2005.

Assireu, A. T., Alcântara, E., Novo, E. M. L. M., Roland, F., Pacheco, F. S., Stech, J. L., and Lorenzzetti, J. A.: Hydro-physical processes at the plunge point: an analysis using satellite and in situ data, Hydrol. Earth Syst. Sci., 15, 3689-3700, doi: 10.5194/hess-15-3689-2011, 2011.

Bailey, T. C., and Gatrell, A. C.: Interactive spatial data analysis, in, Essex: Longman Scientific & Technical, 1995.

Barros, N., Cole, J. J., Tranvik, L. J., Prairie, Y. T., Bastviken, D., Huszar, V. L. M., del Giorgio, P., and Roland, F.: Carbon emission from hydroelectric reservoirs linked to reservoir age and latitude, Nat Geosci, 4, 593-596, doi: 10.1038/Ngeo1211, 2011.

Borges, A. V., Vanderborght, J.-P., Schiettecatte, L. S., Gazeau, F., Ferrón-Smith, S., Delille, B., and Frankignoulle, M.: Variability of the gas transfer velocity of CO_2 in a macrotidal estuary (the Scheldt), Estuaries, 27, 593-603, doi: 10.1007/BF02907647, 2004.

Branco, C. W. C., Rocha, M. I. A., Pinto, G. F. S., Gômara, G. A., and Filippo, R.: Limnological features of Funil Reservoir (R.J., Brazil) and indicator properties of rotifers and cladocerans of the zooplankton community, Lakes Reserv. Res. Manag., 7, 87-92, doi: 10.1046/j.1440-169X.2002.00177.x, 2002.

Butman, D., and Raymond, P. A.: Significant efflux of carbon dioxide from streams and rivers in the United States, Nat Geosci, 4, 839-842, 10.1038/ngeo1294, 2011.

Câmara, G., Souza, R. C. M., Freitas, U. M., and Garrido, J.: Spring: Integrating remote sensing and gis by object-oriented data modelling, Computers & Graphics, 20, 395-403, doi: 10.1016/0097-8493(96)00008-8, 1996.

Cardoso, S. J., Vidal, L. O., Mendonça, R. F., Tranvik, L. J., Sobek, S., and Roland, F.: Spatial variation of sediment mineralization supports differential CO_2 emissions from a tropical hydroelectric reservoir, Frontiers in Microbiology, 4, 10.3389/fmicb.2013.00101, 2013.

Casulli, V., and Cheng, R. T.: Semiimplicit Finite-Difference Methods for 3-Dimensional Shallow-Water Flow, Int J Numer Meth Fl, 15, 629-648, doi: 10.1002/fld.1650150602, 1992.

Cole, J. J., and Caraco, N. F.: Atmospheric exchange of carbon dioxide in a low-wind oligotrophic lake measured by the addition of SF6, Limnol Oceanogr, 43, 647-656, 1998.

Corcos, G. M., and Sherman, F. S.: The mixing layer: deterministic models of a turbulent flow, J Fluid Mech, 139, 29-65, 2005.

Demarty, M., Bastien, J., and Tremblay, A.: Annual follow-up of gross diffusive carbon dioxide and methane emissions from a boreal reservoir and two nearby lakes in Quebec, Canada, Biogeosciences, 8, 41-53, doi: 10.5194/bg-8-41-2011, 2011.

Di Siervi, M. A., Mariazzi, A. A., and Donadelli, J. L.: Bacterioplankton and phytoplankton production in a large Patagonian reservoir (Republica Argentina), Hydrobiologia, 297, 123-129, 1995.

Downing, J. A., Cole, J. J., Middelburg, J. J., Striegl, R. G., Duarte, C. M., Kortelainen, P., Prairie, Y. T., and Laube, K. A.: Sediment organic carbon burial in agriculturally eutrophic impoundments over the last century, Global Biogeochem Cy, 22, Artn Gb1018, doi: 10.1029/2006gb002854, 2008.

Fearnside, P. M., and Pueyo, S.: Greenhouse-gas emissions from tropical dams, Nature Clim. Change, 2, 382-384, 2012.

Finlay, K., Leavitt, P. R., Wissel, B., and Prairie, Y. T.: Regulation of spatial and temporal variability of carbon flux in six hard-water lakes of the northern Great Plains, Limnol Oceanogr, 54, 2553-2564, doi: 10.4319/lo.2009.54.6_part_2.2553, 2009.

Finlay, K., Leavitt, P. R., Patoine, A., and Wissel, B.: Magnitudes and controls of organic and inorganic carbon flux through a chain of hard-water lakes on the northern Great Plains, Limnol Oceanogr, 55, 1551-1564, doi: 10.4319/lo.2010.55.4.1551, 2010.

Fischer, H. B., List, E. J., Koh, R. C. Y., Imberger, J., and Brooks, N. H.: Mixing in inland and coastal waters, Academic Press, New York, 483 pp., 1979.

Fischer, H. B., and Smith, R. D.: Observations of transport to surface waters from a plunging inflow to Lake Mead, Limnol Oceanogr, 28, 258-272, 1983.

Ford, D. E.: Reservoir Transport Processes, in: Reservoir Limnology: Ecological Perspectives, edited by: Thornton, K. W., Kimmel, B. L., and Payne, F. E., Wiley-Interscience, New York, 15-41, 1990.

Gippel, C. J.: The use of turbidimeters in suspended sediment research, Hydrobiologia, 176, 465-480, 10.1007/bf00026582, 1989.

Halbedel, S., and Koschorreck, M.: Regulation of CO_2 emissions from temperate streams and reservoirs, Biogeosciences, 10, 7539-7551, doi: 10.5194/bg-10-7539-2013, 2013.

Hodges, B. R., Imberger, J., Saggio, A., and Winters, K. B.: Modeling basin-scale internal waves in a stratified lake, Limnol Oceanogr, 45, 1603-1620, 2000.

IBGE: Instituto Brasileiro de Geografia e Estatística. Censo Demográfico 2010, Rio de Janeiro, 2010.

Imberger, J., and Patterson, J. C.: Physical Limnology, Adv Appl Mech, 27, 303-475, 1990.

Jahne, B., Munnich, K. O., Bosinger, R., Dutzi, A., Huber, W., and Libner, P.: On the parameters influencing air-water gas-exchange, J Geophys Res-Oceans, 92, 1937-1949, doi: 10.1029/JC092iC02p01937, 1987.

Jin, K., Hamrick, J., and Tisdale, T.: Application of Three-Dimensional Hydrodynamic Model for Lake Okeechobee, Journal of Hydraulic Engineering, 126, 758-771, doi: 10.1061/(ASCE)0733-9429(2000)126:10(758), 2000.

Kelly, C. A., Fee, E., Ramlal, P. S., Rudd, J. W. M., Hesslein, R. H., Anema, C., and Schindler, E. U.: Natural variability of carbon dioxide and net epilimnetic production in the surface waters of boreal lakes of different sizes, Limnol Oceanogr, 46, 1054-1064, 2001.

Kemenes, A., Forsberg, B. R., and Melack, J. M.: CO_2 emissions from a tropical hydroelectric reservoir (Balbina, Brazil), J Geophys Res-Biogeo, 116, Artn G03004, doi: 10.1029/2010jg001465, 2011.

Kennedy, R. H.: Reservoir design and operation: limnological implications and management opportunities, in: Theoretical reservoir ecology and its applications, edited by: Tundisi, J. G., and Straškraba, M., Backhuys Publishers, Leiden, 1-28, 1999.

Klapper, H.: Water quality problems in reservoirs of Rio de Janeiro, Minas Gerais and Sao Paulo, Int Rev Hydrobiol, 83, 93-101, 1998.

Lauster, G. H., Hanson, P. C., and Kratz, T. K.: Gross primary production and respiration differences among littoral and pelagic habitats in northern Wisconsin lakes, Can J Fish Aquat Sci, 63, 1130-1141, doi: 10.1139/f06-018, 2006.

Leonard, B. P.: The Ultimate Conservative Difference Scheme Applied to Unsteady One-Dimensional Advection, Comput Method Appl M, 88, 17-74, doi: 10.1016/0045-7825(91)90232-U, 1991.

Lorenzzetti, J. A., Stech, J. L., Assireu, A. T., Novo, E. M. L. D., and Lima, I. B. T.: SIMA: a near real time buoy acquisition and telemetry system as a support for limnological studies., in: Global warming and hydroelectric reservoirs., edited by: Santos, M. A., and Rosa, L. P., COPPE, Rio de Janeiro, 71-79, 2005.

MacIntyre, S., Jonsson, A., Jansson, M., Aberg, J., Turney, D. E., and Miller, S. D.: Buoyancy flux, turbulence, and the gas transfer coefficient in a stratified lake, Geophys Res Lett, 37, L24604, 10.1029/2010GL044164, 2010.

Martin, J. L., and McCutcheon, S. C.: Hydrodynamics and Transport for Water Quality Modeling, CRC Press, Boca Raton, 1998.

Millero, F. J., Pierrot, D., Lee, K., Wanninkhof, R., Feely, R., Sabine, C. L., Key, R. M., and Takahashi, T.: Dissociation constants for carbonic acid determined from field measurements, Deep-Sea Res Pt I, 49, 1705-1723, doi: 10.1016/s0967-0637(02)00093-6, 2002.

Ometto, J. P., Cimbleris, A. C. P., dos Santos, M. A., Rosa, L. P., Abe, D., Tundisi, J. G., Stech, J. L., Barros, N., and Roland, F.: Carbon emission as a function of energy generation in hydroelectric reservoirs in Brazilian dry tropical biome, Energ Policy, 58, 109-116, doi: 10.1016/j.enpol.2013.02.041, 2013.

Ometto, J. P. H. B., Pacheco, F. S., Cimbleris, A. C. P., Stech, J. L., Lorenzzetti, J., Assireu, A. T., Santos, M. A., Matvienko, B., Rosa, L. P., Sadigisgalli, C., Donato, A., Tundisi, J. G., Barros, N. O., Mendonca, R., and Roland, F.: Carbon Dynamic and Emissions in Brazilian Hydropower Reservoirs, in: Energy Resources: Development, Distribution and Exploitation, edited by: Alcantara, E., Nova Science Publishers, Hauppauge, 155-188, 2011.

Pacheco, F. S., Assireu, A. T., and Roland, F.: Drifters tracked by satellite applied to freshwater ecosystems: study case in Manso Reservoir, in: New technologies for the monitoring and study of large hydroelectric reservoirs and lakes, edited by: Alcantara, E. H., Stech, J. L., and Novo, E. M. L. M., Parêntese, Rio de Janeiro, 193-218, 2011.

Pacheco, F. S., Roland, F., and Downing, J. A.: Eutrophication reverses whole-lake carbon budgets, Inland Waters, 4, 41-48, doi: 10.5268/iw-4.1.614, 2014.

Rangel, L. M., Silva, L. H. S., Rosa, P., Roland, F., and Huszar, V. L. M.: Phytoplankton biomass is mainly controlled by hydrology and phosphorus concentrations in tropical hydroelectric reservoirs, Hydrobiologia, 693, 13-28, doi: 10.1007/s10750-012-1083-3, 2012.

Richardot, M., Debroas, D., Jugnia, L. B., Tadonleke, R., Berthon, L., and Devaux, J.: Changes in bacterial processing and composition of dissolved organic matter in a newly-flooded reservoir (a three-year study), Arch Hydrobiol, 148, 231-248, 2000.

Rocha, M. I. A., Branco, C. W. C., Sampaio, G. F., Gômara, G. A., and de Filippo, R.: Spatial and temporal variation of limnological features, Microcystis aeruginosa and zooplankton in a eutrophic reservoir (Funil Reservoir, Rio de Janeiro), Acta Limnol. Bras., 14, 73-86, 2002.

Roehm, C., and Tremblay, A.: Role of turbines in the carbon dioxide emissions from two boreal reservoirs, Quebec, Canada, J Geophys Res-Atmos, 111, 9, doi: 10.1029/2006jd007292, 2006.

Roland, F., Vidal, L. O., Pacheco, F. S., Barros, N. O., Assireu, A., Ometto, J. P. H. B., Cimbleris, A. C. P., and Cole, J. J.: Variability of carbon dioxide flux from tropical (Cerrado) hydroelectric reservoirs, Aquat Sci, 72, 283-293, doi: 10.1007/s00027-010-0140-0, 2010.

Rosa, L. P., dos Santos, M. A., Matvienko, B., dos Santos, E. O., and Sikar, E.: Greenhouse gas emissions from hydroelectric reservoirs in tropical regions, Climatic Change, 66, 9-21, doi: 10.1023/B:Clim.0000043158.52222.Ee, 2004.

Serra, T., Vidal, J., Casamitjana, X., Soler, M., and Colomer, J.: The role of surface vertical mixing in phytoplankton distribution in a stratified reservoir, Limnol Oceanogr, 52, 620-634, 2007.

Slater, P. G.: Remote sensing, optics and optical systems, Addison-Wesley Pub. Co., Reading, 575 pp., 1980.

Smith, S. V.: Physical, chemical and biological characteristics of CO_2 gas flux across the air water interface, Plant Cell Environ., 8, 387-398, doi: 10.1111/j.1365-3040.1985.tb01674.x, 1985.

Soares, M. C. S., Marinho, M. M., Huszar, V. L. M., Branco, C. W. C., and Azevedo, S. M. F. O.: The effects of water retention time and watershed features on the limnology of two tropical reservoirs in Brazil, Lakes Reserv. Res. Manag., 13, 257-269, doi: 10.1111/j.1440-1770.2008.00379.x, 2008.

Soares, M. C. S., Marinho, M. M., Azevedo, S. M. O. F., Branco, C. W. C., and Huszar, V. L. M.: Eutrophication and retention time affecting spatial heterogeneity in a tropical reservoir, Limnologica - Ecology and Management of Inland Waters, 42, 197-203, doi: 10.1016/j.limno.2011.11.002, 2012.

Spigel, R. H., and Imberger, J.: The Classification of Mixed-Layer Dynamics in Lakes of Small to Medium Size, J Phys Oceanogr, 10, 1104-1121, doi: 10.1175/1520-0485(1980)010<1104:Tcomld>2.0.Co;2, 1980.

St Louis, V. L., Kelly, C. A., Duchemin, E., Rudd, J. W. M., and Rosenberg, D. M.: Reservoir surfaces as sources of greenhouse gases to the atmosphere: A global estimate, Bioscience, 50, 766-775, 2000.

Staehr, P. A., Christensen, J. P. A., Batt, R. D., and Read, J. S.: Ecosystem metabolism in a stratified lake, Limnol Oceanogr, 57, 1317-1330, 10.4319/lo.2012.57.5.1317, 2012.

Stevenson, M. R., Lorenzzetti, J. A., Stech, J. L., and Arlino, P. R. A.: SIMA - An Integrated Environmental Monitoring System, VII Simpósio Brasileiro de Sensoriamento Remoto, Curitiba, 10-14 May, 1993.

Straškraba, M.: Retention time as a key variable of reservoir limnology, in: Theoretical reservoir ecology and its applications, edited by: Tundisi, T. G., and Straškraba, M., Backhuys Publishers, Leiden, 43–70, 1990.

Teodoru, C. R., Prairie, Y. T., and del Giorgio, P. A.: Spatial Heterogeneity of Surface CO_2 Fluxes in a Newly Created Eastmain-1 Reservoir in Northern Quebec, Canada, Ecosystems, 14, 28-46, doi: 10.1007/s10021-010-9393-7, 2011.

Thorpe, S. A., and Jiang, R.: Estimating internal waves and diapycnal mixing from conventional mooring data in a lake, Limnol Oceanogr, 43, 936-945, 1998.

Verburg, P., and Antenucci, J. P.: Persistent unstable atmospheric boundary layer enhances sensible and latent heat loss in a tropical great lake: Lake Tanganyika, J Geophys Res-Atmos, 115, Artn D11109, doi: 10.1029/2009jd012839, 2010.

Vidal, J., Marce, R., Serra, T., Colomer, J., Rueda, F., and Casamitjana, X.: Localized algal blooms induced by river inflows in a canyon type reservoir, Aquat Sci, 74, 315-327, doi: 10.1007/s00027-011-0223-6, 2012.

Wan, Z.: New refinements and validation of the MODIS Land-Surface Temperature/Emissivity products, Remote Sens Environ, 112, 59-74, http://dx.doi.org/10.1016/j.rse.2006.06.026, 2008.

Wan, Z., and Dozier, J.: A generalized split-window algorithm for retrieving land-surface temperature from space, IEEE Trans. Geosci. Remote Sens., 34, 892-905, 10.1109/36.508406, 1996.

Wanninkhof, R.: Relationship between wind-speed and gas-exchange over the ocean, J Geophys Res-Oceans, 97, 7373-7382, doi: 10.1029/92jc00188, 1992.

Weiss, R. F.: Carbon dioxide in water and seawater: the solubility of a non-ideal gas, Marine Chemistry, 2, 203-215, 1974.

Wetzel, R. G., and Likens, G. E.: Limnological Analyses, Springer, New York, 2000.

Wüest, A., and Lorke, A.: Small-scale hydrodynamics in lakes, Annu Rev Fluid Mech, 35, 373-412, doi: 10.1146/annurev.fluid.35.101101.161220, 2003.

Zhao, Y., Wu, B. F., and Zeng, Y.: Spatial and temporal patterns of greenhouse gas emissions from Three Gorges Reservoir of China, Biogeosciences, 10, 1219-1230, doi: 10.5194/bg-10-1219-2013, 2013.

Table 1. Average CO_2 fluxes (mmol m^{-2} d^{-1}) calculated using spatial and temporal data. Positive fluxes denotes net gas fluxes from the lake to the atmosphere. In the last column different letters represent significant differences (t-test, $p < 0.05$). Small letters represent differences between the fluxes in the reservoir zones and capital letters represent the differences between the fluxes in the seasons.

		CO_2 fluxes mmol m^{-2} d^{-1}				
		k_{600} (MacIntyre et al. 2010)		k_{600} (Cole & Caraco 1998)		
		Average	Std. Dev.	Average	Std. Dev.	Significant differences
	Area (km^2)	Spatialized data				
Rainy - Summer						
Entire Reservoir	36.0	-10.1	26.8	-7.2	21.9	
Riverine Zone	5.7	44.5	6.5	37.6	5.5	a
Transition Zone	9.3	-24.8	15.3	-19.1	11.7	b, e
Lacustrine Zone	20.9	-18.3	9.1	-14.1	7.0	b
Dry - Winter						
Entire Reservoir	34.3	24.6	61.5	22.1	50.8	
Riverine Zone	13.7	93.0	13.3	78.7	11.2	c
Transition Zone	7.6	-4.7	51.5	-2.0	42.1	d
Lacustrine Zone	13.1	-29.7	18.1	-22.9	13.9	e
		At the Dam				
All data over the year		-0.1	39.8	-0.9	33.1	
Rainy - Spring		-28.6	24.6	-27.1	18.5	A
Rainy - Summer		8.1	41.8	7.6	35.6	B
Dry - Autumn		23.7	39.2	19.6	29.9	C
Dry - Winter		-0.4	33.0	-0.6	25.5	D

1 Table 2. Average and standard deviation of environmental and chemical variable from the station
2 S28 (near the dam) and river. *Cumulative precipitation over three months

3

Months	Oct-Dec		Jan-Mar		Apr-Jun		Jul-Sep	
Season	Rainy - Autumn		Rainy - Summer		Dry - Spring		Dry - Winter	
	Average	Std. Dev.	Average	Std. Dev.	Average	Std. Dev.	Average	Std. Dev.
Air temperature (°C)	22.5	4.0	24.0	3.3	20.7	3.1	19.6	4.0
Alkalinity (mg L^{-1} as $CaCO_3$)	11.0	0.2	15.5	4.6	11.3	3.7	12.5	3.0
Chlorophyll (mg L^{-1})	12.9	12.8	23.8	20.6	3.0	0.2	23.2	35.0
Total Phosphorus (μg L^{-1})	42.3	8.5	41.7	12.2	18.4	8.6	33.7	28.0
Total Nitrogen (μg L^{-1})	1264.6	357.1	1143.2	305.3	1505.6	454.3	1203.3	299.7
Maximum Depth (m)	65.1	1.8	69.3	1.4	71.6	2.5	69.1	4.4
Mean Reservoir Depth (m)	19.3	0.4	20.3	0.4	20.9	0.7	20.3	1.1
pCO_2 (μatm)	68.9	118.6	848.9	1027.5	1111.8	907.5	521.9	618.5
Precipitation (mm)*	547.0		420.2		230.2		71.6	
Retention Time (days)	27.9	7.7	33.0	9.0	36.4	6.4	33.2	7.4
Max Daily Solar Radiation (W m^{-2})	937.7	276.1	958.1	246.8	716.9	227.2	758.0	189.7
Surface Water temperature (°C)	24.7	1.1	27.1	1.0	24.1	1.7	22.0	1.0
Wind Speed (m s^{-1})	-	-	1.6	1.2	1.4	1.3	1.6	1.5
River Total Phosphorus (mg L^{-1})	80.6	-	77.1	-	42.4	-	88.3	-
River Total Nitrogen (mg L^{-1})	1535.5	-	2072.5	-	1524.2	-	1972.6	-
River Total Carbon (mg L^{-1})	12.9	2.0	13.3	1.8	13.7	2.5	12.1	2.9
Downstream Total Carbon (mg L^{-1})	12.4	2.3	11.8	0.3	13.7	2.6	11.9	1.6
Inflow (m^3 s^{-1})	224.2	58.9	236.4	74.1	234.1	36.7	168.9	28.7
Outflow (m^3 s^{-1})	223.6	57.2	236.4	74.1	226.0	30.9	219.1	10.7

* Cumulative precipitation over three months

4

5

Table 3. Profile's average of the hourly river temperature collected by thermistor chain located at station S05 on 29 February 2012 (rainy season) and 20 September 2012 (dry season).

rainy season					
Hour (LT)	River Temp. (°C)		Hour (LT)	River Temp. (°C)	
	Average	Std. Dev.		Average	Std. Dev.
00:00	28.39	0.04	12:00	27.71	0.03
01:00	28.28	0.04	13:00	27.72	0.04
02:00	28.17	0.05	14:00	27.79	0.11
03:00	28.07	0.03	15:00	27.97	0.06
04:00	28.00	0.02	16:00	28.03	0.02
05:00	27.91	0.04	17:00	28.16	0.09
06:00	27.85	0.04	18:00	28.34	0.09
07:00	27.77	0.05	19:00	28.49	0.06
08:00	27.73	0.00	20:00	28.63	0.04
09:00	27.72	0.01	21:00	28.70	0.01
10:00	27.71	0.02	22:00	28.67	0.03
11:00	27.69	0.01	23:00	28.55	0.05
Max	28.70 (21:00 h)				
Min	27.69 (11:00 h)				

dry season					
Hour (LT)	River Temp. (°C)		Hour (LT)	River Temp. (°C)	
	Average	Std. Dev.		Average	Std. Dev.
00:00	23.90	0.02	12:00	23.80	0.08
01:00	23.88	0.02	13:00	23.82	0.02
02:00	23.80	0.06	14:00	23.87	0.04
03:00	23.74	0.04	15:00	23.89	0.04
04:00	23.71	0.04	16:00	24.00	0.04
05:00	23.66	0.01	17:00	23.97	0.05
06:00	23.64	0.01	18:00	23.99	0.08
07:00	23.60	0.04	19:00	24.08	0.02
08:00	23.57	0.03	20:00	24.03	0.02
09:00	23.59	0.01	21:00	24.00	0.02
10:00	23.62	0.02	22:00	23.96	0.02
11:00	23.65	0.02	23:00	23.95	0.02
Max	24.08 (19:00 h)				
Min	23.57 (08:00 h)				

Table 4. Comparison between CO_2 fluxes (mmol m^{-2} d^{-1}) calculated in periods of low retention time and high retention time. Positive fluxes denotes net gas fluxes from the lake to the atmosphere. The statistical analyses showed significant differences between temporal and spatial data and between low and high retention time (t-test, $p < 0.05$).* We considered data for low retention and high retention time when values was less than 25 days and more than 38 days, respectively. The average of the CO_2 fluxes in periods of intermediate retention time was closely to 0 (0.5 mmol m^{-2} d^{-1}).

	CO2 fluxes mmol m^{-2} d^{-1}			
	Low retention time		High retention Time	
	Average	Std. Dev.	Average	Std. Dev.
Temporal data	-18.6	30.3	14.5	33.6
Spatial data	24.6	61.5	-10.1	26.8

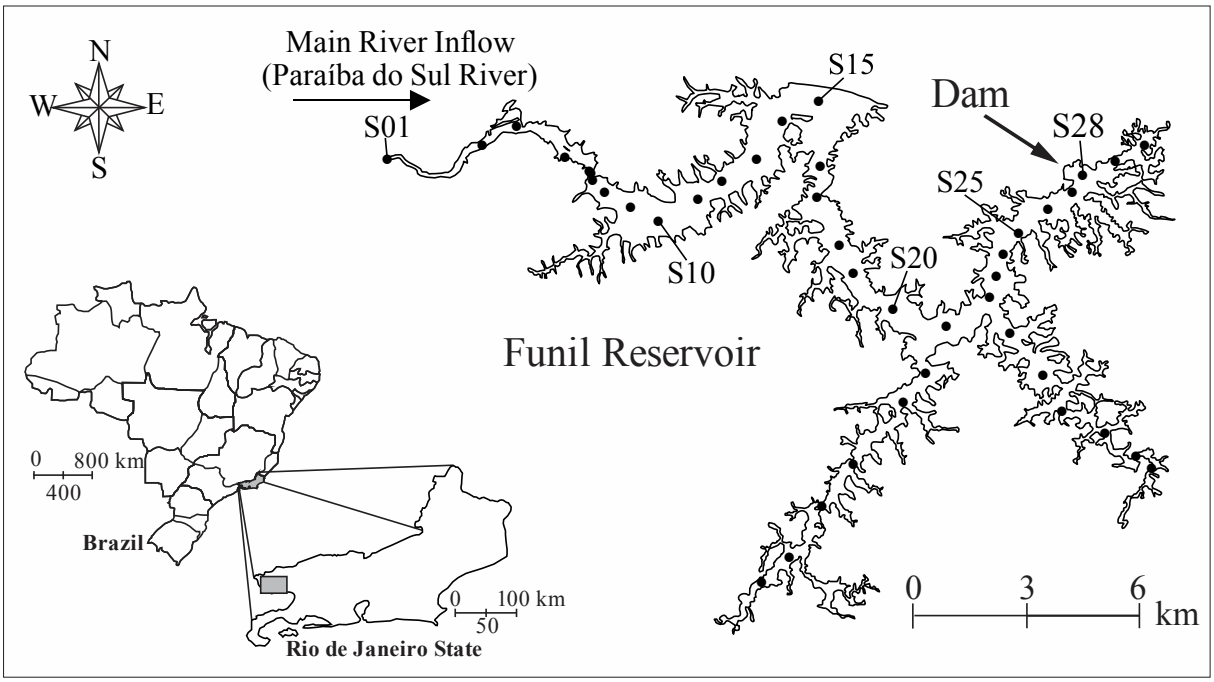

Figure 1. Map of Funil reservoir showing geographic location and sampling stations.

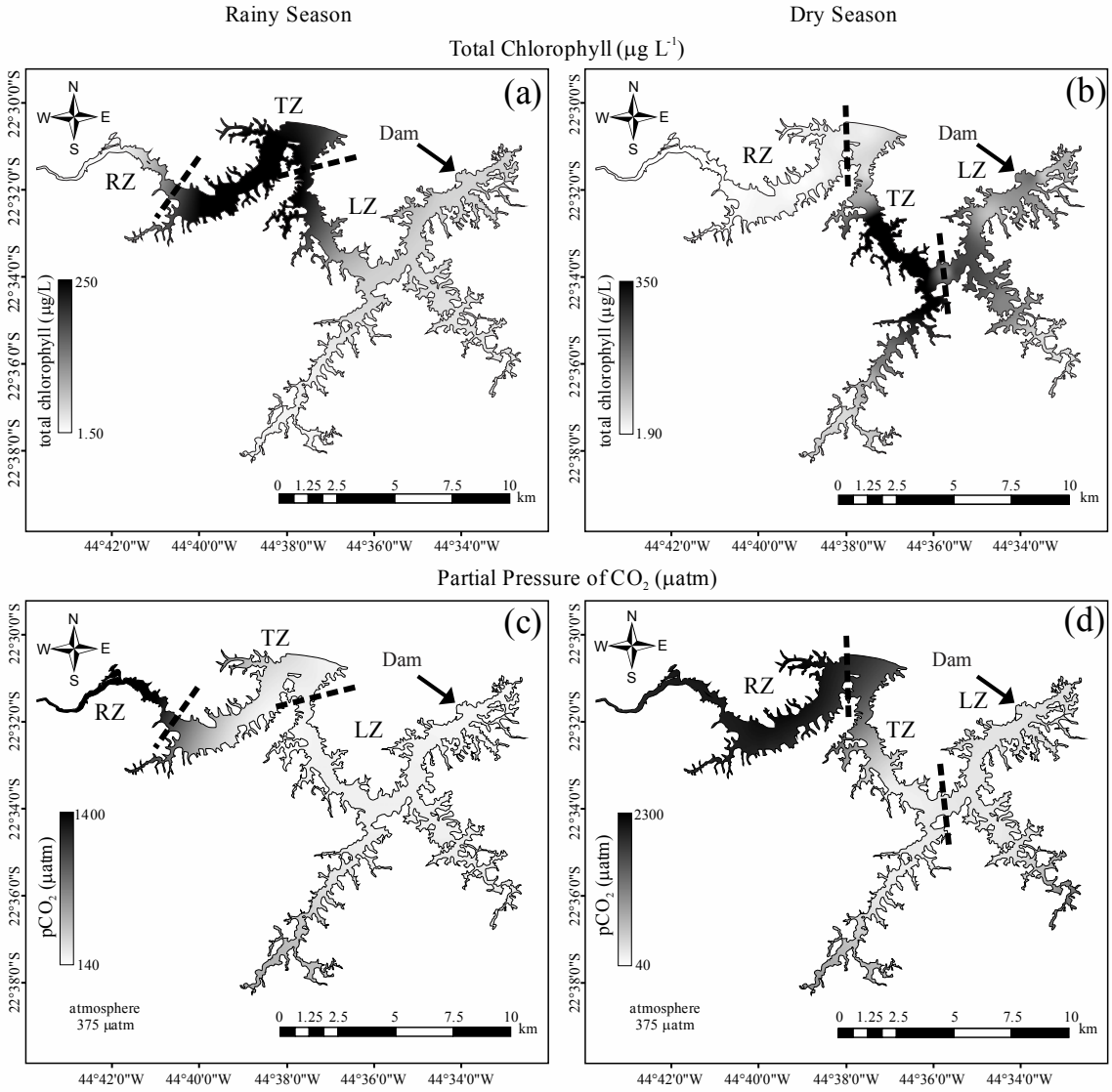

Figure 2. Map of pCO_2 and Chl expressed by a color gradient obtained from interpolation of measured data using the Ordinary Kriging statistical procedures. The root mean-square error (RMSE) of the Kriging prediction calculated comparing observed and calculated values was 90 µatm and 15 µg L^{-1} for pCO_2 and Chl, respectively. Lighter gray represent low Chl (a, b) and low pCO_2 (c, d). RZ = Riverine Zone, TZ = Transition Zone, LZ = Lacustrine Zone.

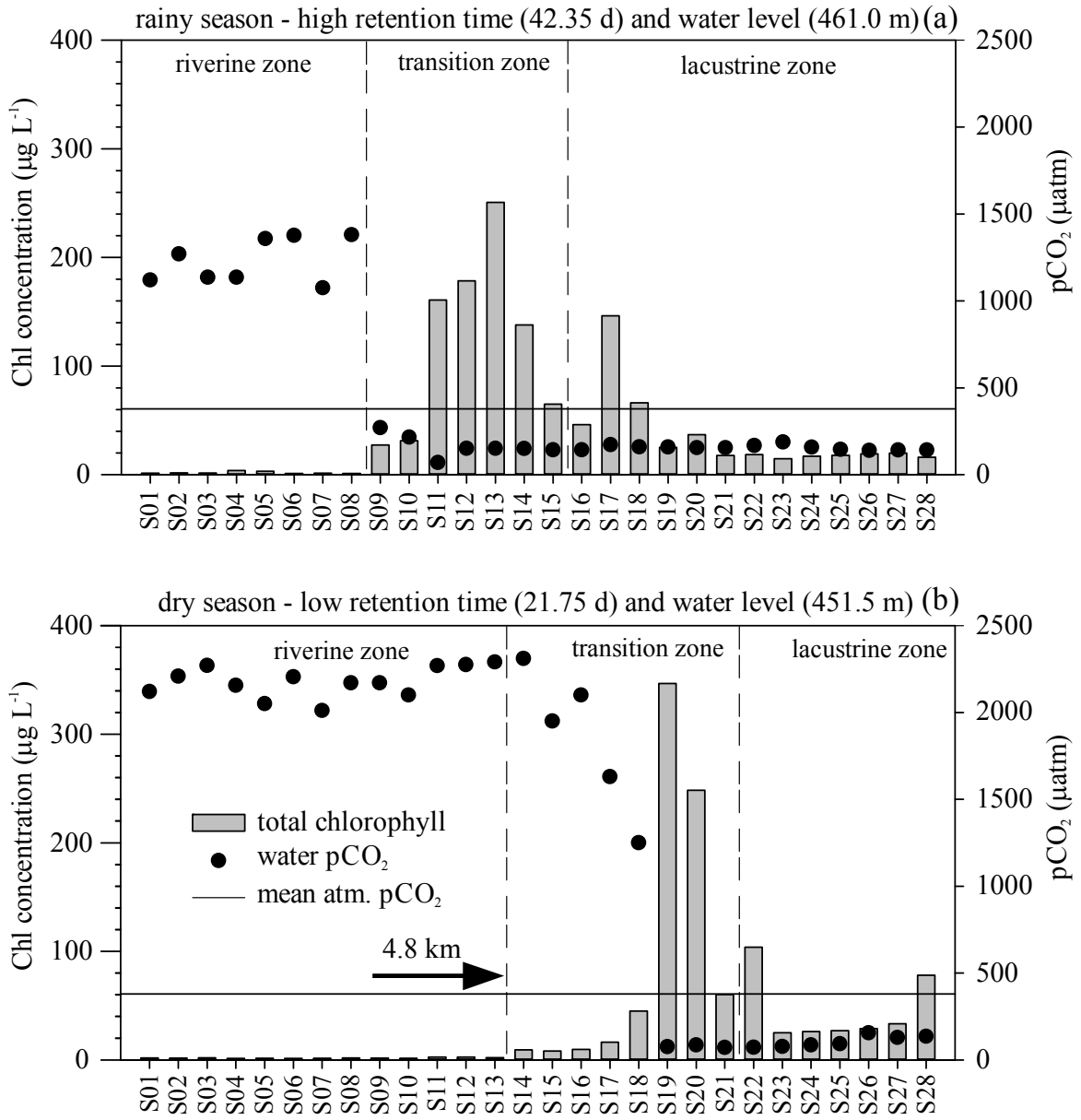

Figure 3. Lotic-lentic gradient of pCO_2 and Chl along the 28 sampling station in the main reservoir body in rainy season (a) and dry season (b). The water level was 461.0 and 451.5 in rainy season and dry season. Three zones can clearly be defined (riverine, transition and lacustrine zone). The arrow shows that the transition zone starts 4.8 kilometers down-reservoir in the period of low water level.

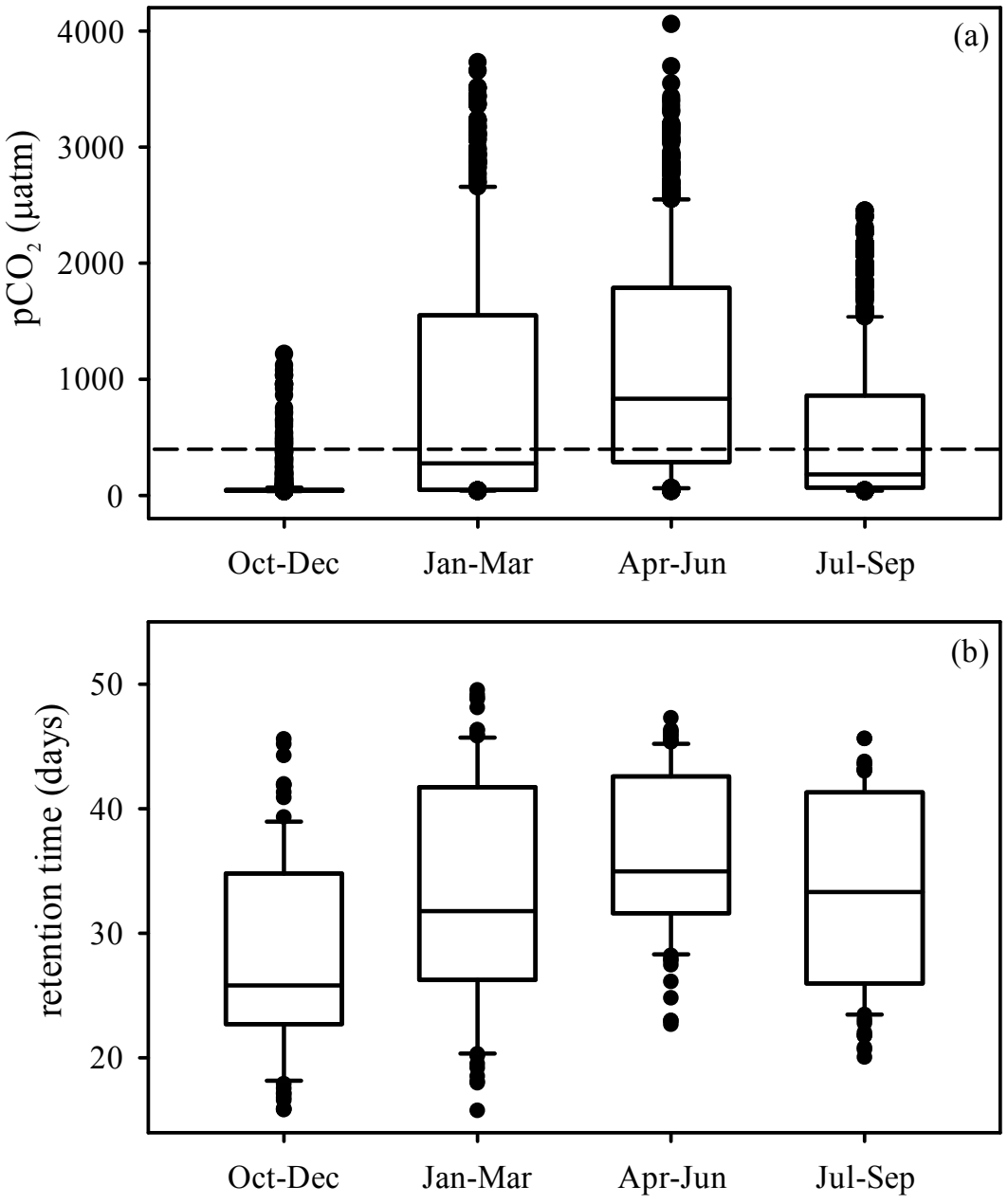

Figure 4. Box plot of pCO_2 at station S28 near the dam (a) and mean reservoir retention time (b) over the studied year. The dashed line represents the average of pCO_2 in the atmosphere (375 µatm). The data are subdivided in four seasons: rainy-spring (Oct-Dec), rainy-summer (Jan-Mar), dry autumn (Apr-Jun) and dry winter (Jul-Sep).

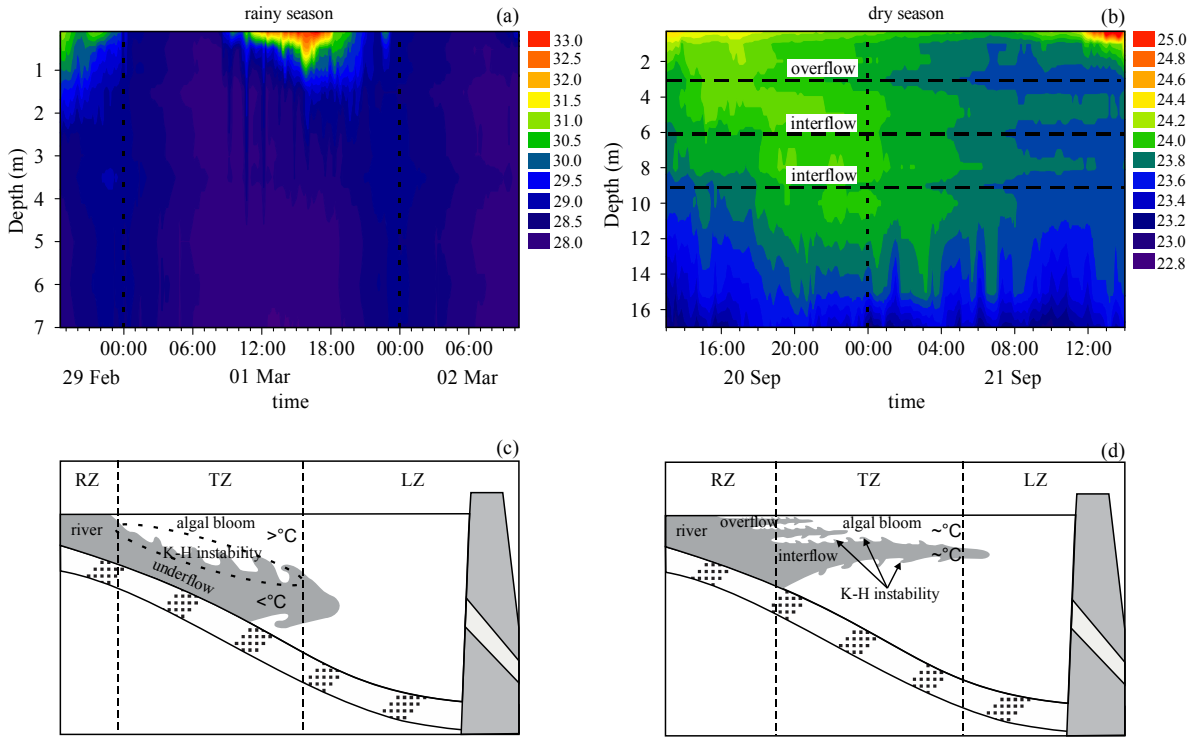

Figure 5. Temperature profile collected at station S09 in rainy season (a) and at station S14 in dry season (b). Dashed line represent the depths where river flows as overflow or interflows. In rainy season the river plunges and flows under the reservoir (underflow) due to difference of density (c). Waves and billows develops along the interface due to shear velocity (Kelvin-Helmholtz instability) and facilitate vertical mixing (see text). In dry season the river flows as overflow or interflow (d) since the difference of density between river and reservoir is low. At this situation, the river can influence the reservoir surface water more 5 kilometers toward the dam. RZ = Riverine Zone, TZ = Transition Zone, LZ = Lacustrine Zone.

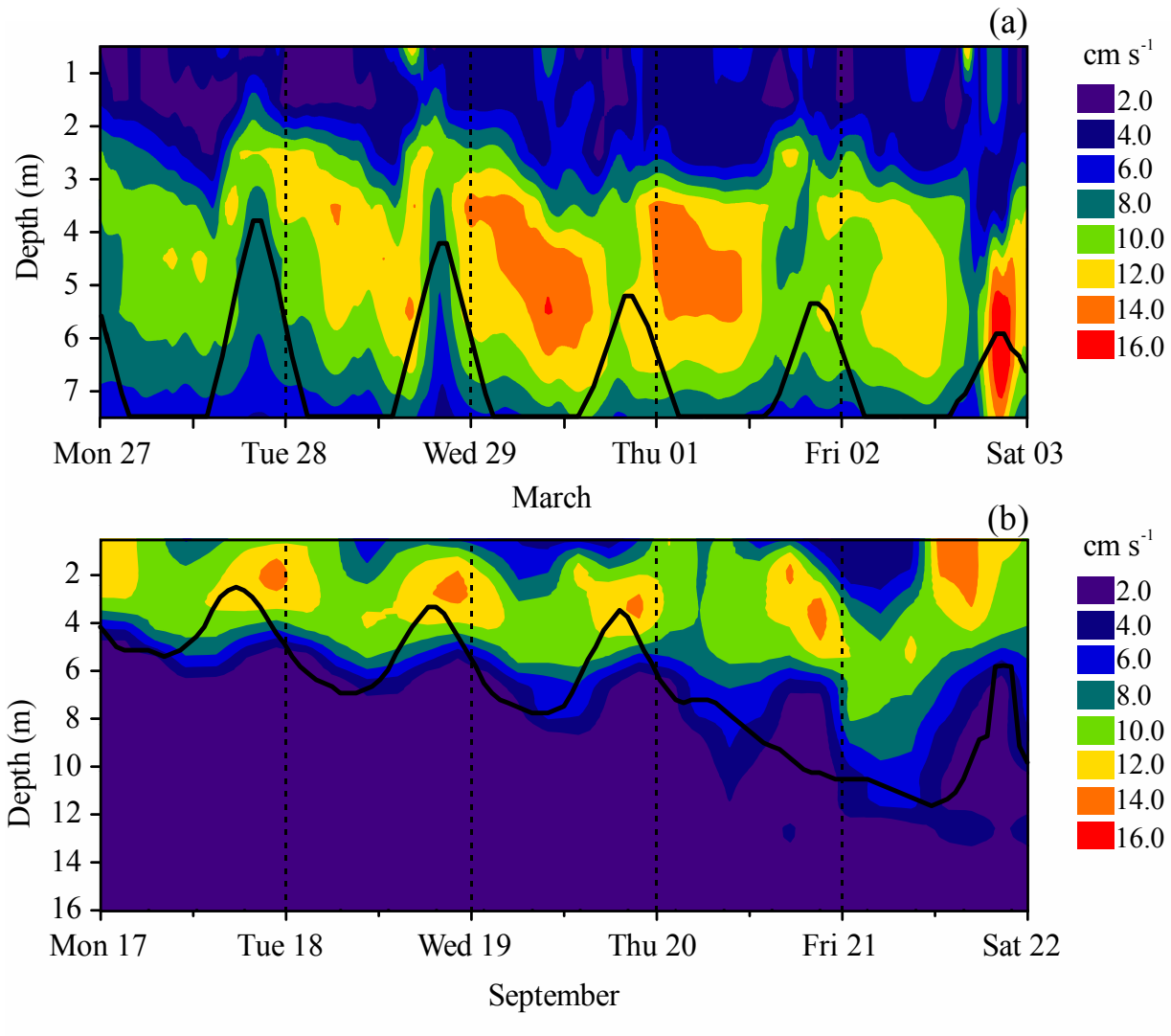

Figure 6. Simulated velocity profile using realistic forcing. Higher velocities represent the depth where the river flows though the transition zone. The river flows as underflow in rainy season when a denser (colder) river plunges beneath the surface and it will flow downward along the bottom as a gravity-driven density current (a). The river flows as overflow in dry season when temperature from river and reservoir are similar (b). As overflow, the river characteristics can be found many kilometers toward the dam at surface water. The black line represents the depth of neutral buoyancy estimated from temperature records, presuming that lake and river water do not mix. The anomaly observed in the river flow and depth of neutral buoyancy between 20 and 21 September 2012 occurred due to a decrease of the river temperature during a rainfall that occurred around 16:00 on 20 September.

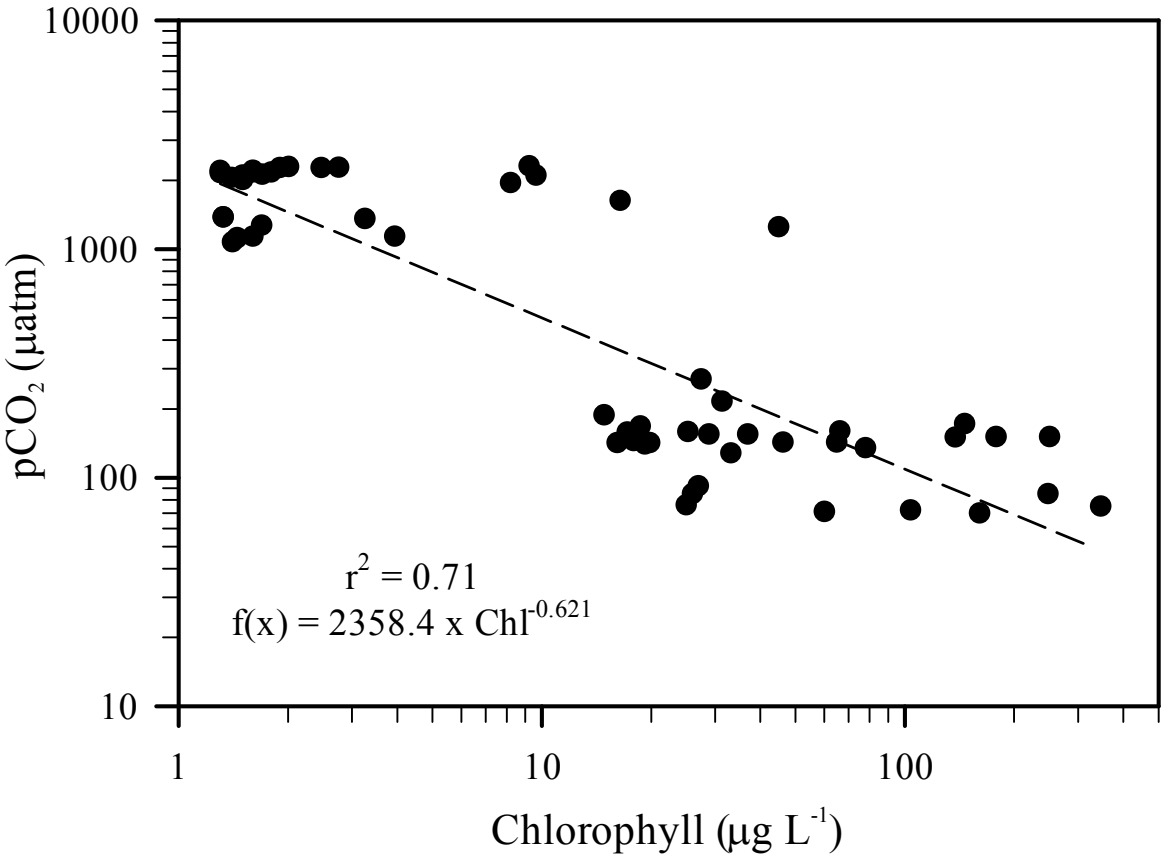

Figure 7. Relationship between spatial data of pCO_2 and Chl in Funil Reservoir. The regression is represented by dashed line ($r^2 = 0.71$, $p < 0.001$).